Journal of Power Sources 449 (2020) 227479

Contents lists available at ScienceDirect

Journal of Power Sources

journal homepage: www.elsevier.com/locate/jpowsour

The ex-situ and in-situ gas diffusivities of polymer electrolyte membrane fuel cell catalyst layer and contribution of primary pores, secondary pores, ionomer and water to the total oxygen diffusion resistance

Sina Salari [a], Mickey Tam [b], Claire McCague [a], Juergen Stumper [b], Majid Bahrami [a,*]

[a] Laboratory for Alternative Energy Conversion (LAEC), School of Mechatronic Systems Engineering, Simon Fraser University, 250-13450 102 Avenue, Surrey, BC, V3T 0A3, Canada

[b] Structure, Properties and Performance Research Division, Automotive Fuel Cell Cooperation Corporation, 9000 Glenlyon Pkwy, Burnaby, BC, V5J 5J8, Canada

HIGHLIGHTS

- Diffusion resistance of pores in CL accounts for about 20% of the total resistance.
- The ionomer-water diffusivity is linearly dependent on primary pore' diameter in CL.
- Porosity of CL affects ionomer-water diffusivity by power of three.
- Secondary pore size effect on ionomer-water diffusivity is negligible.
- Processing procedure of CL could highly affect CL gas diffusivity.

ARTICLE INFO

Keywords:
PEM fuel cells
Catalyst layer
Ex-situ gas diffusivity
In-situ gas diffusivity
Ionomer-water diffusion resistance

ABSTRACT

Oxygen transfer resistance in catalyst layer (CL) of polymer electrolyte membrane fuel cells (PEMFCs) is the limiting factor under high current density operation. The gas diffusivity of the CL has been studied ex-situ and in-situ in the literature, however, an order of magnitude difference between values of ex-situ and in-situ diffusivities and contribution of pores, ionomer and water to the total mass transfer are yet remain to be investigated. In this study ex-situ and in-situ gas diffusion of ten different CL designs are measured. The ex-situ measured resistance is a part of the total resistance measured in-situ, and having that, the constituting parts of total diffusion may be obtained. The diffusion resistance of ionomer-water accounts for about 80% of the total resistance, and the rest is almost all due to secondary pores. Although, primary pores' direct contribution to the diffusion resistance is negligible, their size has a notable impact on the ionomer-water relative diffusivity and increasing their diameter can linearly increase the ionomer-water diffusivity. Moreover, porosity of CL affects ionomer-water diffusivity by power of three. This study shows the efforts to reduce the total oxygen diffusion resistance should focus on increasing the CL porosity and size of primary pores.

1. Introduction

Polymer electrolyte membrane fuel cells (PEMFCs) efficiently convert the reaction energy of hydrogen and oxygen to electricity. A membrane electrode assembly (MEA), which makes up the core of PEMFCs, is constructed from multiple layers of microporous materials, including a 7–20 μm thick catalyst layer (CL), where the Oxygen reduction reaction occurs. Oxygen, hydrogen, ions, water, heat, and electrons transport throughout the CL during PEMFC operation, which make these CL transport properties the key parameters affecting PEMFC performance. Among these transport properties, gas diffusion affects the delivery of reactants to reaction sites. Insufficient supply of oxygen to the CL is a limiting factor to achieve high current densities, and therefore, it is vital to understand and improve the oxygen diffusion rate within CL [1]. The gas diffusion resistance of the gas diffusion layer (GDL) and the electrode (GDL-CL) is higher than the resistance of CL alone, and as a result, their resistance measurement is less challenging than measuring CL resistance alone. As such, there are more available data on GDL [2–4] or GDL-CL electrodes gas diffusion resistance [5]. However, evaluation of gas diffusivity of CL alone remains in demand. Researchers calculated the relative diffusivity of CL based on the

* Corresponding author.
E-mail address: mbahrami@sfu.ca (M. Bahrami).

https://doi.org/10.1016/j.jpowsour.2019.227479
Received 2 June 2019; Received in revised form 9 November 2019; Accepted 16 November 2019
Available online 20 November 2019

Abbreviation

AFCC	Automotive fuel cell cooperation
BJH	Barrett-Joyner-Halenda
CL	Catalyst layer
dm	Dry milling
ETFE	Ethylene tetrafluoroethylene
FIB	Focused ion beam
GDL	Gas diffusion layer
I/C	Ionomer to carbon ratio
MEA	Membrane electrode assembly
MIP	Mercury intrusion porosimetry
MLC	Modified Loschmidt cell
MSP	Method of standard porosimetry
NSERC	Natural Sciences and Engineering Research Council of Canada
PEMFC	Polymer electrolyte membrane fuel cells
PTFE	Polytetrafluoroethylene
PSD	Pore size distribution
SEM	Scan electron microscopy
WKC	Wicke–Kallenbach diffusion cell

Nomenclature

C	Concentration (mol/m^3)
D	Diffusivity (m^2/s)
D^*	Relative diffusivity
d	Diameter (m)
I	Current (amps)
L	Length (m)
M	Molecular weight (kmol/kg)
R	Resistance (s/m)
r	Radius (m)
t	Thickness (m)
F	Faraday constant (C/mol)

Subscripts

d	Drying
eff	effective
ex	Ex-situ
$i\text{-}w$	Ionomer and water
in	In-situ
Kn	Knudsen
lim	Limiting
mt	Mass transfer
np	Pressure independent
pd	Pressure dependent
$prim$	Primary
sec	Secondary

Greek Symbols

γ	Surface tension (N m^{-1})
ε	Porosity
θ	Angle in circular coordinate system (rad)
ρ	Density (kg m^{-3})

reconstructed geometry of CL [6–12]. Nevertheless, direct gas diffusivity measurements are still vital to validate such studies and ensure accuracy. Yu and Carter [13] measured in-plane diffusivity of CL ex-situ using a Wicke–Kallenbach diffusion cell (WKC) and evaluated the effect of ionomer to carbon ratio (I/C) and humidity on CL diffusivity. CL does not exist as a standalone for through-plane gas diffusion measurements and should be coated on a suitable porous substrate, which makes the measurement more challenging than in-plane direction. However, as most likely in PEMFC the gas transports in the through-plane direction to get to the reaction sites in CL, studies on through-plane direction are necessary as well. The support substrate has to be: i) mechanically strong to support the CL, ii) porous enough to let the gas pass through, and iii) with low resistance in the same range as CL (2–10 μm thick porous layer with porosity ≅ 40–70%). Moreover, the combination of the substrate and coating method should result in a uniform CL, without any penetration of CL into the support porous substrate. Inoue et al. [7] used WKC to study the effect of different I/C ratios (0.4–1.4) and carbon support types (Black Pearls, Ketjenblack, and graphitized Ketjenblack with CL porosity ranging from 41% to 75%), on gas diffusivity. The CLs were spray-coated with thicknesses ranging from 22 to 50 μm. However, there was no mention of the support substrate. Shen et al. [14] used a modified Loschmidt cell (MLC) to measure through-plane gas diffusivity of spray-coated CLs on an alumina substrate. As they noticed CL penetration into the hydrophilic substrate, they measured different CL thicknesses gas diffusivity to eliminate the effect of interfacial resistance. The gas diffusivity of CL as a part of the MEA was measured in-situ in Refs. [15–20]. However, these measurements include the gas diffusivity through ionomer and water as well (more details can be found in Ref. [21]), and, as a result, the reported values are several orders of magnitude different than the values reported for ex-situ measurements. The nature of the difference between ex-situ and in-situ gas diffusivities is clear. However, their relationship is not understood and requires a thorough investigation, which is the focus of this study. Moreover, the contribution of each part of CL on the overall mass transfer resistance is analyzed studying both ex-situ and in-situ gas diffusion resistances. Studying ten different CL designs, effect of primary pore diameter, secondary pore diameter, and porosity are studied on the CL ex-situ and in-situ gas diffusivities as well as the ionomer-water gas diffusivity.

2. Experimental methods

2.1. CL composition and processing

The catalyst ink was prepared using catalyst powder consisting of Pt nanoparticles deposited on 10–50 nm partially graphitized carbon particles (50% weight, carbon particle mean diameter equal to 30 nm). Based on the design, the CL powder was dry-milled for 0–48 h in a ceramic jar (US Stoneware, model 755 RMW) containing zirconia balls. To prepare the catalyst ink, after dry milling, the powder was dispersed

Table 1
CL designs I/C, dry milling time, and drying temperature. The porosity is calculated based on measured thickness of CL, and the mean pore diameter is based on measurements done by N_2 adsorption porosimetry and applying Barrett-Joyner-Halenda (BJH) theory.

Design number	1	2	3	4	5	6	7	8	9	10
I/C	1.1	1.1	1.1	1.1	1.1	0.9	0.9	0.9	0.7	0.7
Dry milling (dm) time, hr	48	6	0	0	48	48	24	6	48	24
Drying temperature (T_d), °C	50	50	50	20	20	50	50	50	50	50
Porosity (%)	22	45	58	59	28	43	50	58	46	56
Mean pore diameter (nm)	34	57	66	31	31	35	52	69	35	40

in the solvent which was deionized water and alcohol. Then aqueous ionomer dispersion (Aquivion® PFSA, Solvay) was added. Finally, the ink was placed in the ceramic jar and jar milled for a specific duration. Following previous study [22], CL was coated with Mayer bar on the porous PTFE filters (Fluoropore FHUP04700, EMD Millipore), with 85% porosity and thickness of 50 μm for ex-situ measurements, and dried at different temperatures based on the CL design. The substrate was chosen with a specific surface property (highly hydrophobic) and pore size (<500 nm) to minimize CL penetration. The uniformity of the CL and no penetration of the catalyst ink into the support substrate was confirmed based on the SEM images of the prepared CL samples cross-section in our previous study [22].

For PSD measurements, the same sample preparation was followed except for the support substrate. ETFE sheets were used for CL samples prepared for pore size distribution (PSD) measurements, and then the CL was decal transferred onto Nafion membrane (25 μm NRE211, Chemours) by hot-pressing at 150 °C and 15 bar for 2.5 min. The design parameters for the prepared CL samples are presented in Table 1.

For in-situ measurement of gas diffusion resistance, a custom-built multi-cell hardware with co-flow straight channel design and active area of 40 cm^2 was used. MEA's for each design in Table 1 were made by first transferring the cathode CL from ETFE decals to Gore 0.05 mg/cm^2 Pt loaded anode half-CCM using a hot-press at 150 °C, 15 bar pressure for 3 min. Subsequently, the full-CCM was sandwiched between two Freudenberg GDL's and held together with frames made from Sheldahl PEN film, and the whole MEA was then bonded using a hot-press at 150 °C, 15 bar pressure for 3 min. Three MEA's for each design were tested using the custom hardware on a custom automated test station at high stoich ratios (i.e., greater than 10) to achieve iso-condition throughout the cell.

2.2. CL structural characterization

The thickness of CL was measured using SEM images of CL coated substrates cross-sectioned by a freeze and fracture procedure, and then the porosity was calculated based on the thickness measurement and platinum loading measurements. The details of the methods could be found in Ref. [22]. The measured porosity include both hydrophobic and hydrophilic pores.

To measure the PSD of the CL samples, method of standard porosimetry (MSP), mercury intrusion porosimetry (MIP), analyzing the reconstructed geometry of CL based on FIB-SEM imaging, and N_2 adsorption methods were tried. Comparing results (presented in Ref. [22]) the N_2 adsorption method using BJH theory was chosen.

A volumetric nitrogen physisorption porosimeter (Autosorb iQ-MP, Quantachrome Instruments) was used to measure the isotherms of the CL samples. A 9 mm sample cell with bulb and filler rod was loaded with at least 300 mg of catalyst-coated membrane for each test. The CL samples were dried under vacuum for over 10 h at 50 °C. The sample cell was then immersed in liquid nitrogen, and nitrogen adsorption and desorption isotherms were collected. A total of 200 data points were collected for each isotherm and each test was repeated at least three times.

2.3. Gas diffusion measurement

Following Fick's law of diffusion (Eq. (1)) Binary gas diffusivity D_{binary} is the diffusion coefficient for a system of two gases in an open space.

$$N = -D_{binary}\frac{\partial C}{\partial x} \tag{1}$$

where N is the mass flux, C is concentration. When diffusion happens through a porous media the diffusion coefficient is the effective diffusivity of porous media D_{eff}.

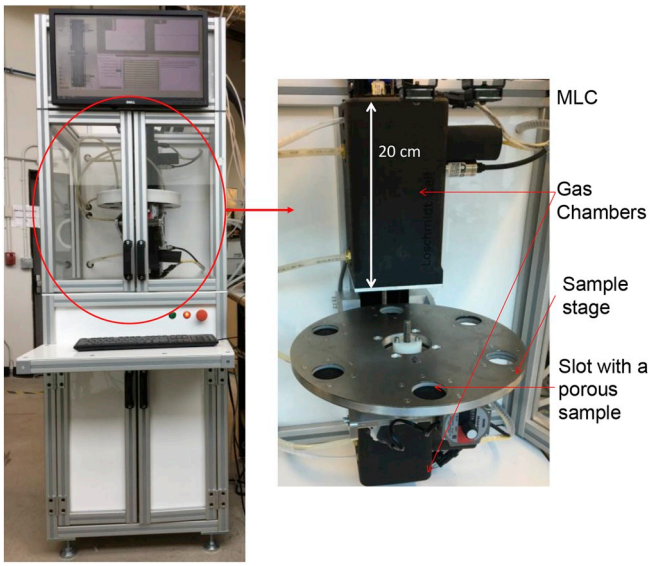

Fig. 1. Our custom-designed Modified Loschmidt Cell (MLC) test bed for the ex-situ measurements.

The relative diffusivity of a porous sample is the ratio of its effective diffusivity and the binary diffusivity:

$$D^{*} = \frac{D_{eff}}{D_{\text{binary}}} \tag{2}$$

Diffusion resistance of a sample which is a quantitative property is defined as the ratio of the sample thickness over its diffusivity:

$$R = \frac{l}{D_{eff}} \tag{3}$$

where l is the thickness. Effective diffusion length L_{eff} is equivalent to diffusion resistance and defined as the ratio of diffusion resistance and binary diffusion coefficient:

$$L_{eff} = \frac{R}{D_{binary}} \tag{4}$$

The ex-situ gas diffusion measurements were performed using an MLC testbed (Fig. 1). The testbed had two large gas-filled chambers at the same pressure connected by a closed valve and the porous sample sandwiched in between. At time zero each chamber contained one type of gas (oxygen and nitrogen), and then opening the valve, the gases diffused into the other chamber, and the concentration of each one changed with respect to time at any specific location. Comparing the measured gas concentrations during the experiment and using the available analytical solution for this 1-D diffusion problem [23], the gas diffusion resistance of the sample was calculated and related to its relative diffusivity. The detailed explanation of the procedure followed here could be found in our previous study, Ref. [22]. For each design at least 3 samples were measured 10 times each to ensure reproducibility of the results.

Following Baker et al. [20] the effective diffusivity of a PEMFC cathode CL could also be determined in-situ by limiting current measurements (I_{lim}). In this method, the total O_2 mass-transfer resistance (R_{mt}) was defined as the change in O_2 concentration from the channel to the cathode electrode, divided by the average O_2 molar flux to the cathode (in the through-plane direction). At I_{lim} conditions (T = 68 °C, RH = 75%) the O_2 concentration at the cathode electrode was zero, and the O_2 molar flux was equal to the current (measured) divided by a constant (*4 F*). R_{mt} was also equal to the ratio of the effective diffusion length L_{eff} to the effective diffusivity D_{eff}. Therefore, we could obtain D_{eff} from measuring I_{lim} and the thickness of the layer through which the gas

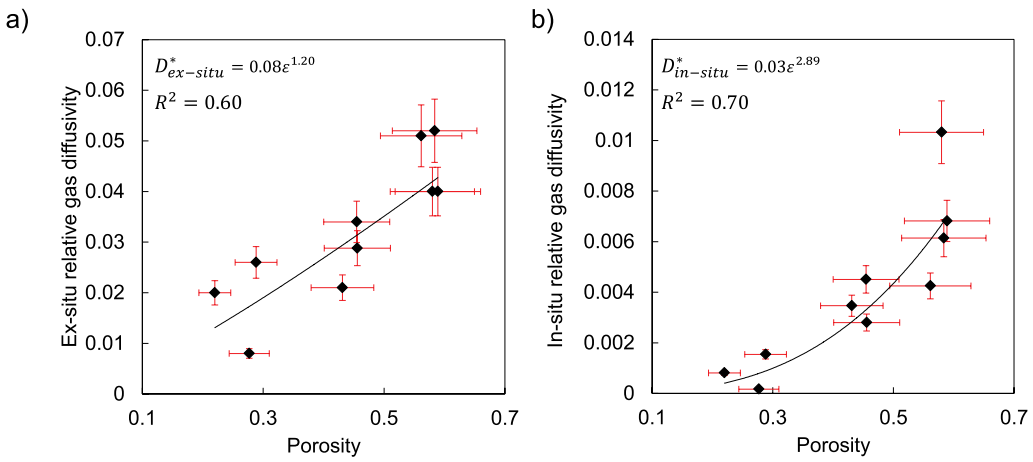

Fig. 2. a) The measured ex-situ and b) in-situ relative gas diffusivities versus porosity. As the standard deviations of repeated measurements for the CL ex-situ relative diffusivity were less than the calculated uncertainties based on the thickness measurements, for both relative diffusivity and porosity, the error bars are calculated based on the thickness measurements uncertainties. However, for in-situ relative diffusivities, the error bars are standard deviations for three repeated measurements.

diffused. Accordingly, the following definition held:

$$R_{mt} = \frac{4 \cdot F \cdot C_{O2-channel}}{I_{lim}} = \frac{L_{eff}}{D_{eff}} \quad (5)$$

Molecular diffusion coefficients (gas-phase transport) were inversely proportional to the total pressure P, while diffusion through small pores ($d < 60$ nm, Knudsen diffusion), and diffusion through ionomer and/or water films covering the Pt nanoparticles were independent of pressure. These properties were exploited to separate R_{mt} into a P-dependent R_{pd} and a P-independent component R_{np}. The plot of R_{mt} vs. P was linear; R_{np} was given by the intercept while R_{pd} was given by the slope times the pressure.

$$R_{mt} = R_{np} + R_{pd}(P) = Intercept + Slope \cdot P \quad (6)$$

R_{pd} was associated with O_2 transport in the channel, in the pores of the GDL, and in the cracks and larger pores of the MPL.

R_{np} was associated to Knudsen diffusion in the MPL and CCL and O_2 diffusion in the ionomer/liquid-water film of the CCL.

The purpose of this procedure was to measure R_{np} and R_{pd} that could be subsequently associated/correlated to structural properties of the pertaining MEA components. R_{np} was equal to the intercept only when the water vapor partial pressure was constant during the measurement. In case, instead, where the RH was constant a correction should be applied to obtain R_{np}.

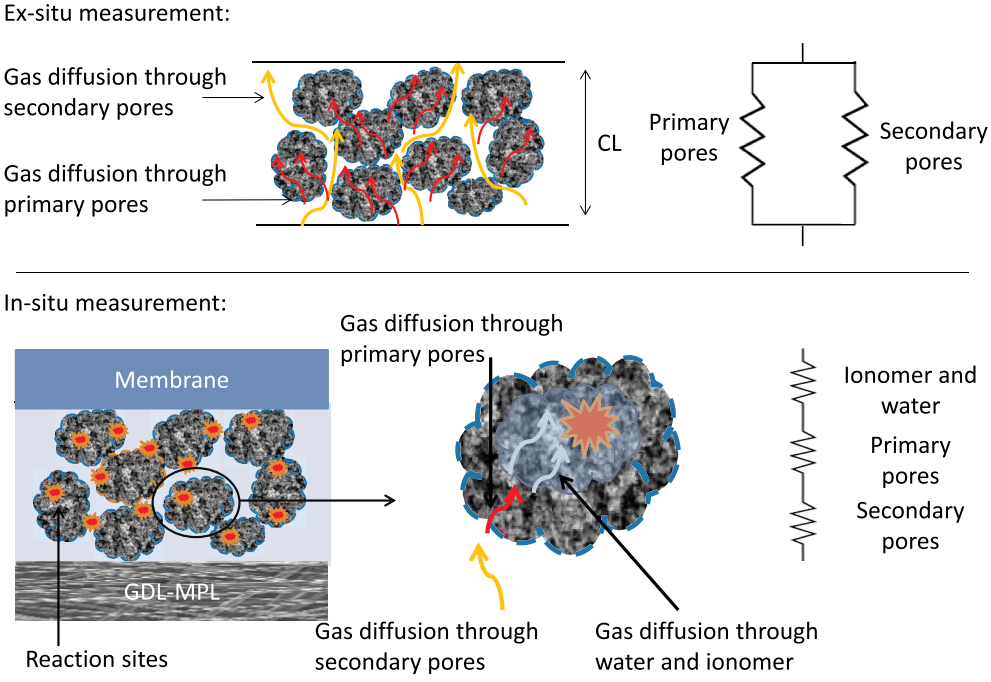

Fig. 3. Ex-situ and in-situ gas diffusion paths and their equivalent resistance network.

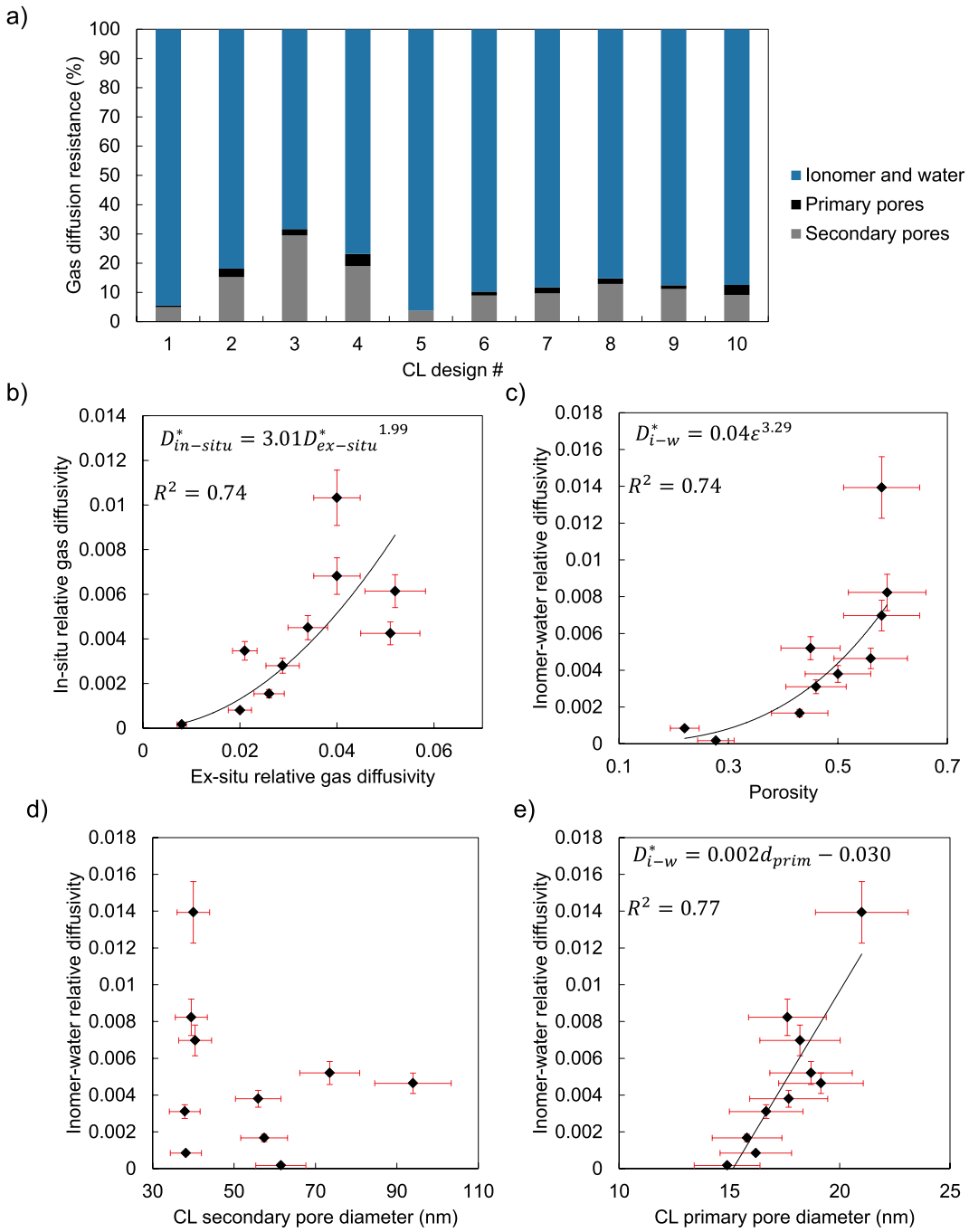

Fig. 4. a) The contribution of ionomer and water, primary and secondary pores to the gas diffusion resistance through CL. The calculated ionomer-water relative diffusivity versus b) the CL ex-situ relative diffusivity, c) the CL porosity, d) the CL secondary pore mean diameter, and e) the CL primary pore mean diameter.

3. Results and discussion

3.1. Ex-situ and in-situ relative gas diffusivities, porosity and pore diameter

Fig. 2a and b show the measured ex-situ and in-situ relative gas diffusivities versus the CL porosities, regardless of the production process. While the general upward dependencies of relative diffusivity to porosity were apparent, there were no simple mathematical functions relating porosity to relative diffusivities. Different production procedures resulted in different PSDs, pore connectivity, and even pore structures, which will be discussed later. As a result, porosity alone could not specify the relative diffusivity values. Such behaviour might seem obvious; however, it is common in the literature to consider the gas diffusivity (and other transport properties) as a function of only porosity (e.g., power function [24]) in the porous media field. In such models, based on the general structure of a material (e.g., a network of cylindrical fibers, agglomerate-type) or experimental data, different constants were fitted for the property function of a substance. Fig. 2a and b show the shortcoming of such functions for the CL. Moreover, a conventional Bruggeman model [24] overestimates the CL relative diffusivity by an order of magnitude in comparison with the measured values for relative diffusivity.

The dependency of the in-situ diffusivity on porosity was more than the ex-situ values (power of 2.9 versus power of 1.2). In-situ diffusivity included the gas diffusion through ionomer, and primary pores within

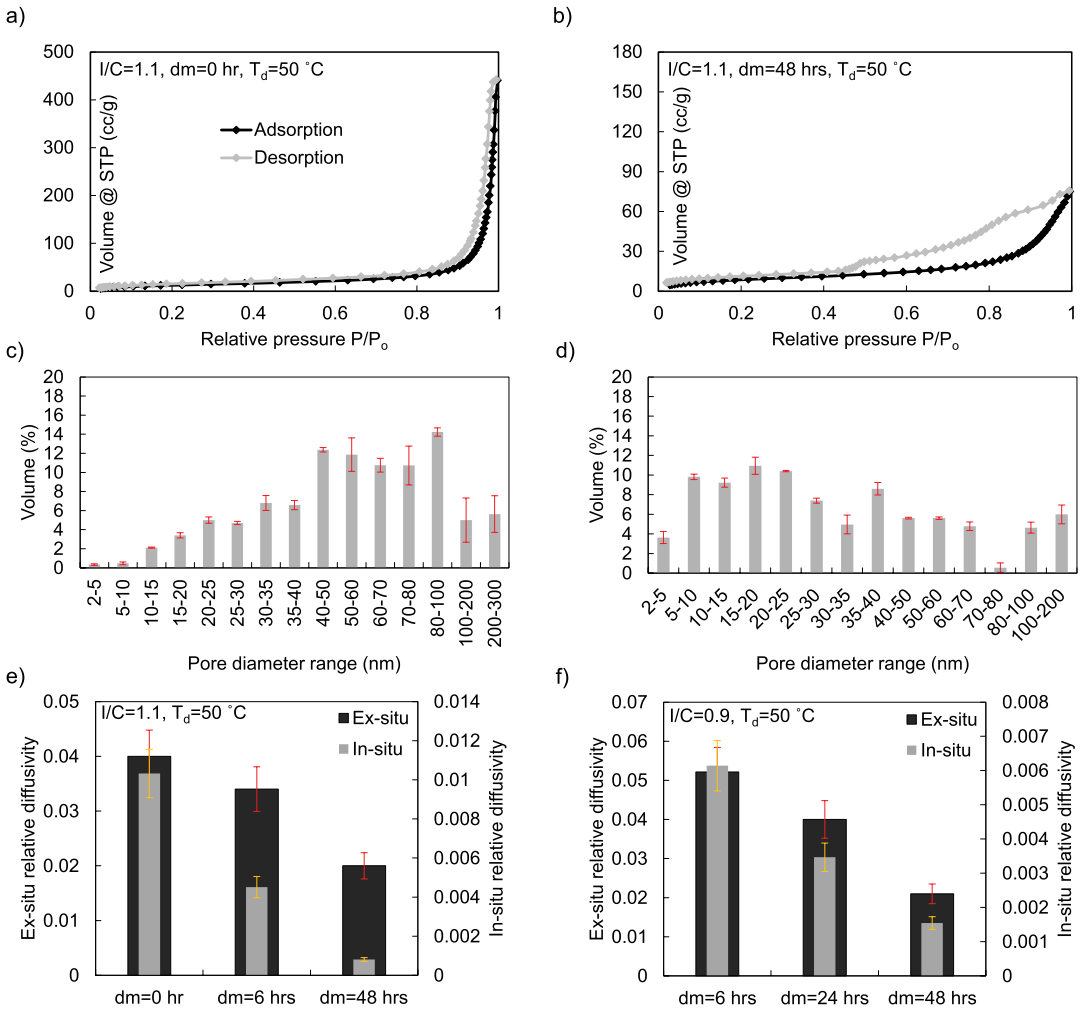

Fig. 5. Isotherms obtained by N_2 adsorption of CL designs with I/C = 1.1, T_d = 50 °C, and a) dm = 0 h, b) dm = 48 h. The measured PSD by N_2 adsorption porosimetry based on BJH theory for CL designs with I/C = 1.1, T_d = 50 °C, and c) dm = 0 h, d) dm = 48 h. The error bars are the standard deviation of 3 measurement repetitions. The measured relative diffusivity values comparison for CL design sets with different dry milling times for CL designs with e) I/C = 0.9 and T_d = 50 °C, and f) I/C = 1.1 and T_d = 50 °C. The error bars are calculated based on the uncertainty of thickness and oxygen concentration measurements.

agglomerates as well as the secondary pores. Higher porosities could result in thinner ionomer/water thicknesses and improved formed-water removal during the operation (The Pt loading density of different samples in this work was kept constant to eliminate effect of difference in Pt loading density on gas diffusivities of different CL designs).

3.2. The gas diffusion resistance contribution of primary pores, secondary pores, ionomer and water through CL

Considering Fig. 3 in ex-situ tests, gas crossed through the secondary and primary pores of CL. The primary and secondary pores mostly acted in parallel and the measured resistance could be related to secondary and primary pores' resistances through Eq. (7):

$$R_{ex-situ}^{-1} = R_{ex-sec}^{-1} + R_{ex-prim}^{-1} \tag{7}$$

where, sec and prim stands for secondary and primary pores, respectively. As the gas diffusivity within primary pores was dominated with Knudsen mechanism it could be calculated using Eq. (8) [25]:

$$D_{prim} = D_{Kn} = (8/3) r_{prim} \sqrt{RT/2\pi M} \tag{8}$$

To calculate the resistance through primary pores, the CL thickness was chosen for the diffusion length, as gas had to pass through the entire CL in ex-situ tests (Fig. 3):

$$R_{ex-prim} = \frac{l_{CL}}{(8/3) r_{prim} \sqrt{RT/2\pi M}} \tag{9}$$

where, l_{CL} is the thickness of CL. The secondary pores resistance was calculated based on the measured ex-situ total resistance, the calculated primary pores resistance Eq. (7), Eq. (9) and Eq. (10):

$$R_{ex-sec} = \left(R_{ex-situ}^{-1} - R_{ex-prim}^{-1}\right)^{-1} = \frac{t_{CL}}{D_{sec}} \tag{10}$$

In in-situ tests, gas had to reach the reaction sites in the vicinity of Pt particles, i.e., it had to diffuse through ionomer, water, and primary pores, as well as secondary pores, and, all of these paths were in series this time (Fig. 3):

$$R_{in-situ} = R_{in-sec} + R_{in-prim} + R_{i-w} \tag{11}$$

where, i-w stands for ionomer and water.

Here the path for oxygen to reach reaction sites is varying from zero for reaction sites on the GDL/MPL-CL interface to the CL thickness for reaction sites at the CL-membrane interface (assuming 1-D diffusion). As a result, following Mench [21] half of the CL thickness was chosen for the diffusion length through secondary pores, i.e., the secondary pore diffusion resistance here was the half of the one measured in ex-situ. For

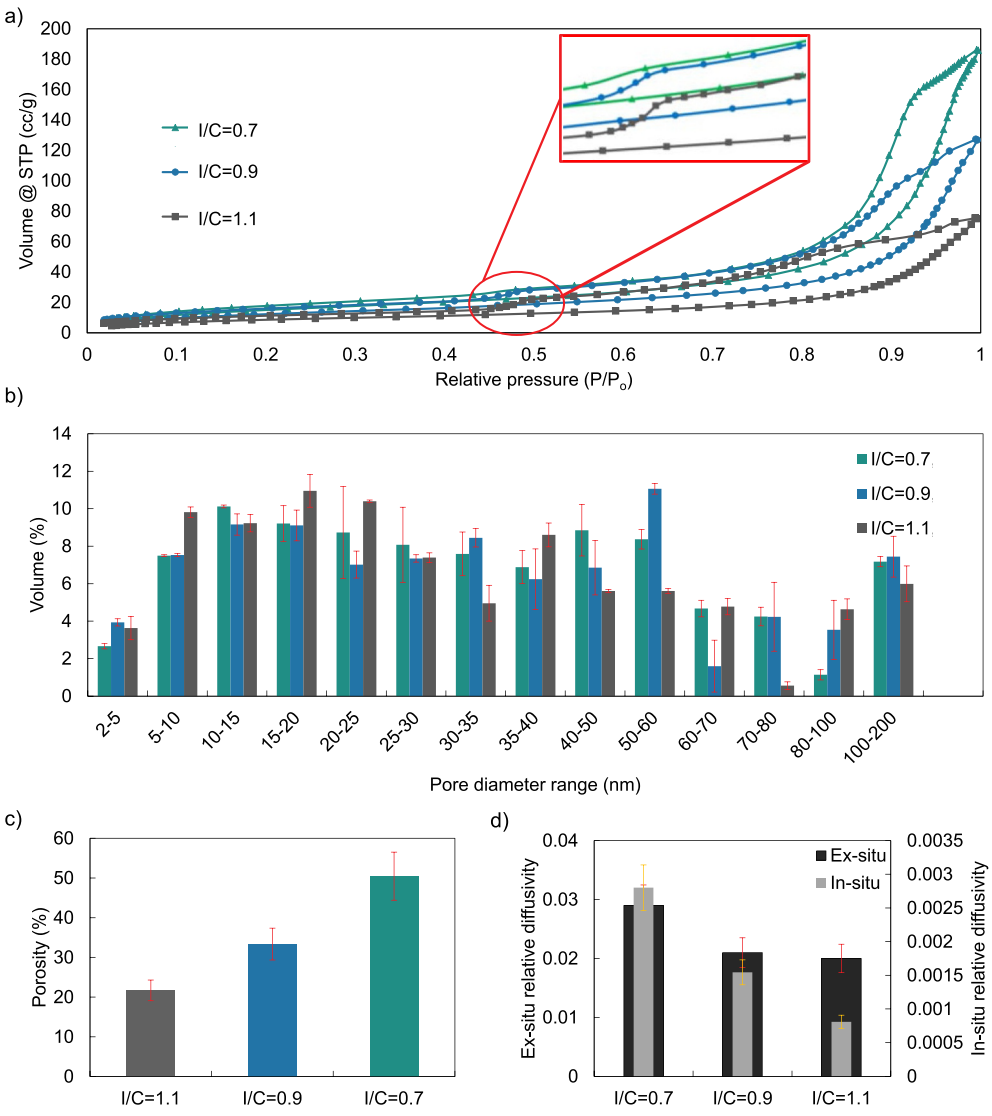

Fig. 6. a) Isotherms obtained by N_2 adsorption porosimetry, b) PSDs obtained by N_2 adsorption porosimetry applying BJH method, c) porosities calculated based on thickness measurements, and d) the measured relative diffusivity values comparison for CL designs with the same dry milling time 48 h, drying temperature 50 °C, and different I/Cs: 0.7, 0.9, and 1.1. The error bars of PSDs and in-situ relative diffusivities show calculated standard deviation for three repeating measurements of the same sample. The error bars of porosity values and ex-situ relative diffusivities were calculated based on thickness and oxygen probe measurement uncertainties.

primary pores, as gas should cross the agglomerates, agglomerates diameter would be a logical choice for the diffusion length. However, measuring agglomerates diameter was challenging. Secondary pores were the gaps between agglomerates and in the same order as the agglomerate size, and N_2 adsorption method is a well-established method to measure pore diameter. As a result, diameter of secondary pores was chosen for the diffusion length through primary pores. Then, Eq. (11) could be rewritten:

$$R_{in-situ} = \frac{t_{0.5CL}}{D_{in-situ}} = \frac{t_{0.5CL}}{D_{ex-sec}} + \frac{d_{sec}}{D_{prim}} + R_{i-w} \tag{12}$$

where, $t_{0.5CL}$ is the half thickness of CL. The diffusivity of primary pores was calculated using Eq. (8). Dividing Eq. (12) by the total mass diffusion resistance (which was the same as in-situ diffusion resistance), the contribution of each CL component to the total gas diffusion resistance could be found:

$$1 = \frac{D_{in-situ}}{D_{ex-sec}} + \frac{D_{in-situ}}{(4/3)d_{prim}\sqrt{RT/2\pi M}}\frac{d_{sec}}{t_{0.5CL}} + \frac{D_{in-situ}R_{i-w}}{t_{0.5CL}} \tag{13}$$

Substituting the values of diffusivities and lengths for different designs, all terms in Eq. (13) could be obtained for all the designs (Fig. 4).

The plot in Fig. 4a shows the dominance part of the gas diffusion limitation is due to ionomer and water. While the primary pores themselves did not contribute much to the gas diffusion resistance directly (because of the short gas passage through them <70 nm), their effect on the ionomer and water resistance was important which will be discussed later. 20% of the gas diffusion resistance was due to the secondary pores in the baseline design #3 which is the design used in industrial fuel cells for automotive applications. This portion of resistance contradict the traditional belief that CL pores gas diffusion resistance is negligible in comparison with ionomer-water part of the resistance.

Fig. 4b shows that the ex-situ and in-situ gas diffusivities were highly related. The ex-situ diffusivity was directly related to the porosity and mean pore diameter of the CL. These two parameters could affect the water/ionomer thickness and water removal procedure inside CL under operation. Such effect could be the main reason for the dependence of the measured relative ex-situ and in-situ diffusivities. To understand the effect of the porosity and pore diameters on the different component of mass transfer resistance, the relative diffusivity of ionomer-water was defined here based on the ionomer-water resistance as follows:

$$D^*_{i-w} = \frac{t_{0.5CL}}{D_{binary}R_{i-w}} \tag{14}$$

Porosity could affect the water distribution and also the connectivity of ionomer network throughout the CL. Both of mentioned effects change the ionomer-water relative diffusivity. Fig. 4c confirms the dependency of the ionomer-water relative diffusivity to porosity. However,

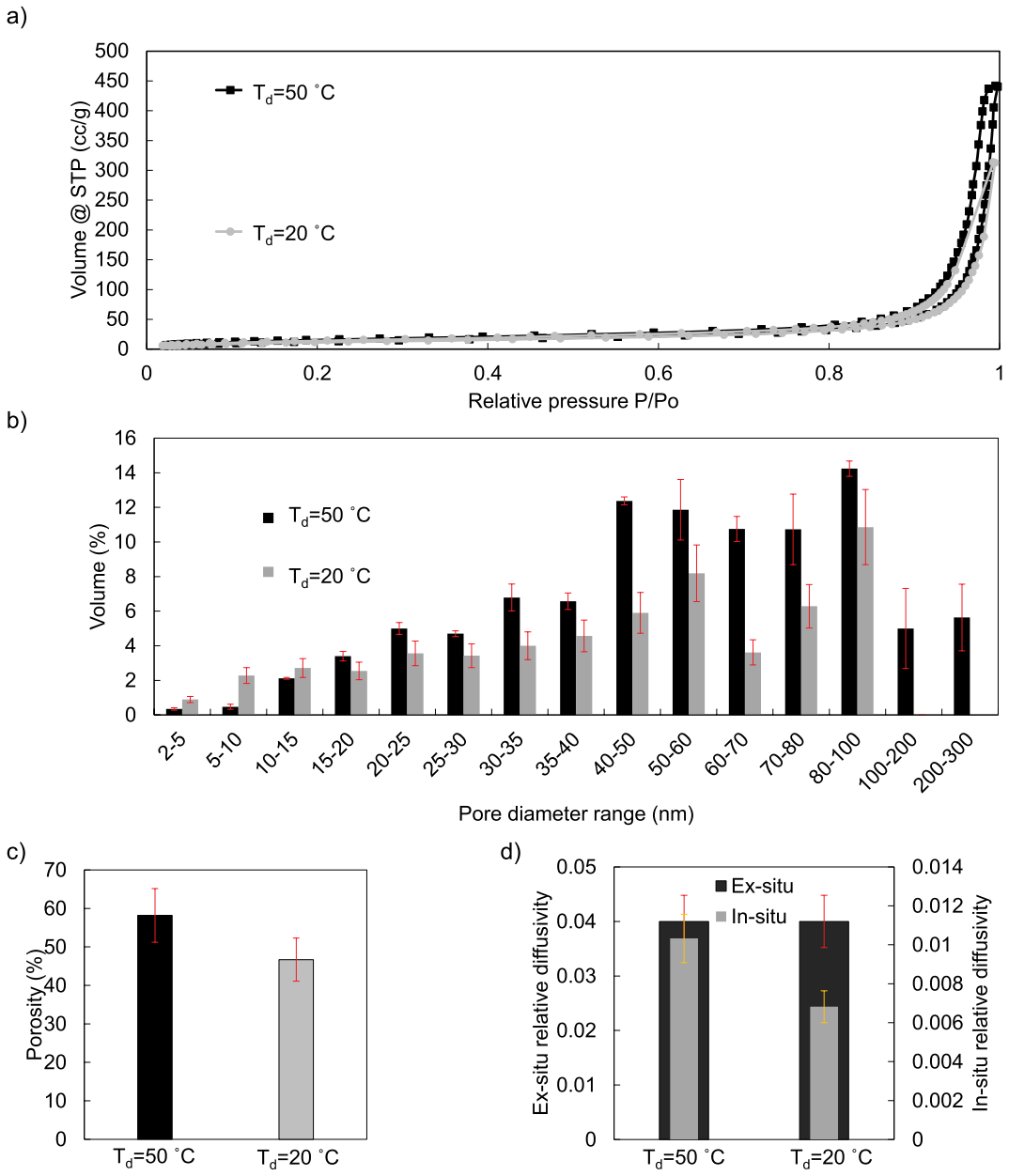

Fig. 7. a) Isotherms obtained by N_2 adsorption porositimetry, b) PSDs obtained by N_2 adsorption porositimetry, c) porosities, and d) ex-situ and in-situ relative gas diffusivity of CL designs with the same I/C = 1.1, dm = 0 h, T_d = 50 °C and 20 °C. The error bars shows calculated standard deviation for 3 repeating measurements of the same sample.

Fig. 4d indicates that the secondary pore diameter did not affect the ionomer-water relative diffusivity, as formed water inside the CL tended to fill the small pores i.e. primary pores, and reactions happened on the triple phase boundaries, where primary pores were the bottle necks not the secondary pores for the access. The fundamental difference between dependency of ionomer-water relative diffusivity to secondary pores and primary pores could be seen comparing Fig. 4d and e. Ionomer-water relative diffusivity was almost a linear function of the primary pore mean diameters which was supported by theory too considering the fact that the ionomer/water thickness would be proportional to the available surface area per volume for it to spread:

$$D_{i-w} \propto \frac{1}{R_{i-w}} \propto \frac{1}{t_{i-w}} \propto \frac{1}{area/volume} \propto \frac{1}{1/d_{characteristic}} \propto d_{characteristic} \quad (15)$$

In Eq. (15), the characteristic diameter is the pore diameters which were filled with ionomer and water. Fig. 4e shows that this characteristic diameter was almost the same as the mean primary pore diameter in the CLs.

3.3. Effect of dry milling (dm) time on the CL structure

Considering the shape of the isotherm for the CL design with I/C = 1.1, dry milling time (dm) = 0 h, Td = 50 °C in Fig. 5a, the isotherm and hysteresis loop are type IV and H1, respectively, based on the International Union of Pure and Applied Chemistry (IUPAC) classification of isotherms [26]. Type IV isotherms indicate the filling and emptying of mesopores by capillary condensation and evaporation, respectively [27], and H1 hysteresis is associated with narrow, uniform pore distribution with open-ended cylindrical shapes. As shown in Fig. 5b, dry milling the CL powder changed the isotherm shape drastically. The hysteresis type of this design was H2 indicating a network of disordered interconnected pores of progressive sizes. The wide hysteresis loop was

due to the pore blocking effects associated with ink-bottle pores [27]. However, the sudden change at P/Po = 0.48 is a well-known flag for cavitation phenomenon which happens when the pore neck diameter is less than 5 nm [28] (the existence of such pores was confirmed later in pore size distribution measurement). Similar transformation in isotherm shape was detected for CL samples with I/C = 0.9 that were dry milled for 6, 24, and 48 h. Moreover, the amount of nitrogen adsorbed decreased for designs with 48 h of dry milling indicating a reduction of pore volume for the range of pore sizes detectable by N_2 adsorption. The same trend for the porosities of CL could be found (see Table 1).

Increasing the dry milling time resulted in a shift in the PSD peak to smaller pores and a reduction of the mean pore diameter (Fig. 5c and d). The results suggest that longer dry milling time created smaller agglomerates and, subsequently CL with smaller pores.

Fig. 5e and f shows the measured relative diffusivities for CL designs with different dry milling times. The sharp drops (around 50%) of the ex-situ relative diffusivities for design sets showed in Fig. 5e and f going from low dry-milled to high dry-milled samples was aligned with the expected effect due to drop in porosity, pore sizes, and more tortuous path for highly dry-milled samples (based on the isotherms in Fig. 5b). The effect of dry milling was in all cases more intense on the in-situ gas diffusivity than the ex-situ gas diffusivity, as in-situ gas diffusivity was mostly function of ionomer-water resistance which as mentioned was a function of primary pore diameter.

3.4. Effect of ionomer to carbon ratio on the CL structure

Fig. 6a shows the isotherms for the CL designs with the same dry milling time 48 h, and drying temperature 50 °C, but, different I/Cs. In all these isotherms the cavitation effect and the volume of the adsorbed nitrogen decreased with increasing I/C. Logically this trend was a result of ionomer acting as a binder. Ionomer mostly filled the secondary pores in CL and did not penetrate into primary pores [29], therefore increasing the ionomer content of CL from 0.7 to 1.1 should result in narrower pore necks i.e., stronger cavitation effect. Also, it would lead to reducing the portion of secondary pores. On the other hand, increasing ionomer content of the CL would block more of primary pores accessible by nitrogen. As a result, although volume portion of pores larger than 20 nm decreased increasing I/C from 0.7 to 1.1, the shape of PSD did not change drastically (Fig. 6b), however, porosity dropped (Fig. 6c). It should be mentioned that in these measurements the volume of pores smaller than 2 nm (pores within carbon particles) was ignored.

The comparison of the measured relative diffusivity values for design sets with different I/Cs (Fig. 6d) was in-line with the calculated porosities and measured PSDs. The effect of ionomer content was again more intense for in-situ diffusivity as porosity drop affects the in-situ relative diffusivity more than ex-situ ones.

3.5. Effect of drying temperature of catalyst ink on the CL structure

Fig. 7a shows the obtained isotherms for CL designs with I/C = 1.1, no dry milling time, and dried at 20 and 50 °C. Drying the CL in the lower temperature slowed down the drying process and let the capillary forces act to settle the CL ink. It resulted in a lower volume of adsorbed nitrogen. The comparison between the PSDs of the CL with different drying temperature (Fig. 7b) shows that lower drying temperature shifted the pore sizes toward the smaller diameters. Although the difference between obtained porosities for CL with different dry millings were in the range of experimental uncertainties (Fig. 7c), lower porosities for designs dried at room temperature were expected.

The in-situ gas diffusivity dropped for CL design dried at 20 °C (Fig. 7d) which was logical considering smaller pore sizes for this design in comparison with the one dried at 50 °C. However, the ex-situ diffusivity was almost the same for both designs. One explanation for the different behaviours of the in-situ and ex-situ relative diffusivities could be the effect of different drying temperatures on the connectivity of pores in secondary pore scale, i.e., drying CL in lower temperature, gave the capillary forces enough time, to form a cluster of connected agglomerates and connected pores surrounding the agglomerates. Further investigation was needed to prove this hypothesis, however, as drying the CLs dried at 20 °C did not perform well, further investigation was eliminated.

4. Conclusions and remarks

An MLC testbed and in-situ limiting current method were used to measure ex-situ and in-situ gas diffusivities of CL of PEMFCs with 10 designs varying I/Cs (1.1, 0.9, 0.7), catalyst powder dry milling time (0, 6, 24, 48 h) and catalyst ink drying temperatures (50 and 20 °C). The following were the major conclusions:

1. Having in-situ and ex-situ gas diffusion resistances, contribution of different components of CL on total gas diffusion resistance could be calculated.
2. Ionomer-water gas diffusion resistance accounted for almost 80% of the total resistance and the rest was due to gas diffusion through secondary pores in CL.
3. Porosity of CL affected ionomer-water gas diffusion resistance to the power of about 3, primary pore diameter was inversely proportional to the ionomer-water gas diffusion resistance, and secondary pores seemed to have no relation to it.
4. Changing porosity, primary and secondary pore diameter sizes, and structural shape of CL were possible through varying ratio of catalyst material or processing procedure of making CL, which could highly affect both in-situ (performance of CL) and ex-situ gas diffusivities, i.e., processing procedure of CL (which got less attention in the literature) could be as important as composition of CL to optimize the performance.

Declaration of competing interest

The authors declare that they have no known competing financial interests or personal relationships that could have appeared to influence the work reported in this paper.

Acknowledgment

This research is supported by funding from the Natural Sciences and Engineering Research Council of Canada (NSERC) Collaborative Research and Development (Grant No. M-CRDPJ453170) and Automotive Fuel Cell Corporation (AFCC). The AFCC Structure, Properties and Performance Research Division is acknowledged for their technical support. This work made use of the 4D LABS shared facilities supported by the Canada Foundation for Innovation (CFI), British Columbia Knowledge Development Fund (BCKDF), Western Economic Diversification Canada (WD), and Simon Fraser University(SFU).

References

[1] G. Inoue, M. Kawase, Effect of porous structure of catalyst layer on effective oxygen diffusion coefficient in polymer electrolyte fuel cell, J. Power Sources 327 (2016) 1–10, https://doi.org/10.1016/j.jpowsour.2016.07.037.
[2] M.S. Ismail, D.B. Ingham, K.J. Hughes, L. Ma, M. Pourkashanian, Effective diffusivity of polymer electrolyte fuel cell gas diffusion layers: an overview and numerical study, Int. J. Hydrogen Energy 40 (2015) 10994–11010, https://doi.org/10.1016/j.ijhydene.2015.06.073.
[3] N. Zamel, N.G.C. Astrath, X. Li, J. Shen, J. Zhou, F.B.G. Astrath, H. Wang, Z.S. Liu, Experimental measurements of effective diffusion coefficient of oxygen-nitrogen mixture in PEM fuel cell diffusion media, Chem. Eng. Sci. 65 (2010) 931–937, https://doi.org/10.1016/j.ces.2009.09.044.
[4] R. Rashapov, F. Imami, J.T. Gostick, A method for measuring in-plane effective diffusivity in thin porous media, Int. J. Heat Mass Transf. 85 (2015) 367–374, https://doi.org/10.1016/j.ijheatmasstransfer.2015.01.101.
[5] J. Zhao, S. Shahgaldi, I. Alaefour, S. Yang, X. Li, Pore structure and effective diffusion coefficient of catalyzed electrodes in polymer electrolyte membrane fuel

cells, Int. J. Hydrogen Energy 43 (2018) 3776–3785, https://doi.org/10.1016/j.ijhydene.2018.01.019.
[6] H. Ostadi, P. Rama, Y. Liu, R. Chen, X.X. Zhang, K. Jiang, 3D reconstruction of a gas diffusion layer and a microporous layer, J. Membr. Sci. 351 (2010) 69–74, https://doi.org/10.1016/j.memsci.2010.01.031.
[7] G. Inoue, K. Yokoyama, J. Ooyama, T. Terao, T. Tokunaga, N. Kubo, M. Kawase, Theoretical examination of effective oxygen diffusion coefficient and electrical conductivity of polymer electrolyte fuel cell porous components, J. Power Sources 327 (2016) 610–621, https://doi.org/10.1016/j.jpowsour.2016.07.107.
[8] S. Litster, W.K. Epting, E.A. Wargo, S.R. Kalidindi, E.C. Kumbur, Morphological analyses of polymer electrolyte fuel cell electrodes with nano-scale computed tomography imaging, Fuel Cells 13 (2013) 935–945, https://doi.org/10.1002/fuce.201300008.
[9] A. Berson, H.W. Choi, J.G. Pharoah, Determination of the effective gas diffusivity of a porous composite medium from the three-dimensional reconstruction of its microstructure, Phys. Rev. E - Stat. Nonlinear Soft Matter Phys. 83 (2011) 1–12, https://doi.org/10.1103/PhysRevE.83.026310.
[10] N.A. Siddique, F. Liu, Process based reconstruction and simulation of a three-dimensional fuel cell catalyst layer, Electrochim. Acta 55 (2010) 5357–5366, https://doi.org/10.1016/j.electacta.2010.04.059.
[11] W. Wu, F. Jiang, Microstructure reconstruction and characterization of PEMFC electrodes, Int. J. Hydrogen Energy 39 (2014) 15894–15906, https://doi.org/10.1016/j.ijhydene.2014.03.074.
[12] H. Fathi, A. Raoof, S.H. Mansouri, Insights into the role of wettability in cathode catalyst layer of proton exchange membrane fuel cell; pore scale immiscible flow and transport processes, J. Power Sources 349 (2017) 57–67, https://doi.org/10.1016/j.jpowsour.2017.03.012.
[13] Z. Yu, R.N. Carter, Measurement of effective oxygen diffusivity in electrodes for proton exchange membrane fuel cells, J. Power Sources 195 (2010) 1079–1084, https://doi.org/10.1016/j.jpowsour.2009.08.065.
[14] J. Shen, J. Zhou, N.G.C. Astrath, T. Navessin, Z.-S. (Simon) Liu, C. Lei, J.H. Rohling, D. Bessarabov, S. Knights, S. Ye, Measurement of effective gas diffusion coefficients of catalyst layers of PEM fuel cells with a Loschmidt diffusion cell, J. Power Sources 196 (2011) 674–678, https://doi.org/10.1016/j.jpowsour.2010.07.086.
[15] K. Wippermann, K. Klafki, A.A. Kulikovsky, In situ measurement of the oxygen diffusion coefficient in the cathode catalyst layer of a direct methanol fuel cell, Electrochim. Acta 141 (2014) 212–215, https://doi.org/10.1016/j.electacta.2014.06.164.
[16] A.A. Kulikovsky, A simple equation for in situ measurement of the catalyst layer oxygen diffusivity in PEM fuel cell, J. Electroanal. Chem. 720–721 (2014) 47–51, https://doi.org/10.1016/j.jelechem.2014.03.005.
[17] S. Sambandam, J. Parrondo, V. Ramani, Estimation of electrode ionomer oxygen permeability and ionomer-phase oxygen transport resistance in polymer electrolyte fuel cells, Phys. Chem. Chem. Phys. 15 (2013) 14994–15002, https://doi.org/10.1039/c3cp51450a.
[18] H. Liu, W.K. Epting, S. Litster, Gas transport resistance in polymer electrolyte thin films on oxygen reduction reaction catalysts, Langmuir 31 (2015) 9853–9858, https://doi.org/10.1021/acs.langmuir.5b02487.
[19] G.S. Hwang, A.Z. Weber, Effective-diffusivity measurement of partially-saturated fuel-cell gas-diffusion layers, J. Electrochem. Soc. 159 (2012) F683–F692, https://doi.org/10.1149/2.024211jes.
[20] D.R. Baker, D.a. Caulk, K.C. Neyerlin, M.W. Murphy, Measurement of oxygen transport resistance in PEM fuel cells by limiting current methods, J. Electrochem. Soc. 156 (2009) B991–B1003, https://doi.org/10.1149/1.3152226.
[21] M. Mench, Introduction to fuel cells, in: Fuel Cell Engines, Wiley-Blackwell, 2008, https://doi.org/10.1002/9780470209769.ch1.
[22] S. Salari, J. Stumper, M. Bahrami, Direct measurement and modeling relative gas diffusivity of PEMFC catalyst layers : the effect of ionomer to carbon ratio , operating temperature , porosity , and pore size distribution, Int. J. Hydrogen Energy 43 (2018) 16704–16718, https://doi.org/10.1016/j.ijhydene.2018.07.035.
[23] Waterloo Technical Instrument, Symmetrical Modified Loschmidt Cell Operator ' S Manual, 2017.
[24] D.A.G. Bruggeman, Berechnung verschiedener physikalischer Konstanten von heterogenen Substanzen. I. Dielektrizitätskonstanten und Leitfähigkeiten der Mischkörper aus isotropen Substanzen, Ann. Phys. 416 (1935) 665–679.
[25] W. Kast, C.R. Hohenthanner, Mass transfer within the gas-phase of porous media, Int. J. Heat Mass Transf. 43 (2000) 807–823, https://doi.org/10.1016/S0017-9310(99)00158-1.
[26] R. Françoise, J. Rouquerol, K. Sing, Adsorption by Powders and Porous Solids, 1999. London.
[27] T. Horikawa, D.D. Do, D. Nicholson, Capillary condensation of adsorbates in porous materials Amount adsorbed, Adv. Colloid Interface Sci. 169 (2011) 40–58, https://doi.org/10.1016/j.cis.2011.08.003.
[28] C.J. Rasmussen, A. Vishnyakov, M. Thommes, B.M. Smarsly, F. Kleitz, A. V Neimark, Cavitation in metastable liquid nitrogen confined to nanoscale pores, Langmuir 26 (2010) 10147–10157, https://doi.org/10.1021/la100268q.
[29] T. Soboleva, X. Zhao, K. Malek, Z. Xie, T. Navessin, S. Holdcroft, On the micro-, meso-, and macroporous structures of polymer electrolyte membrane fuel cell catalyst layers, ACS Appl. Mater. Interfaces 2 (2010) 375–384, https://doi.org/10.1021/am900600y.